ARL-TR-7494 ● SEP 2015

US Army Research Laboratory

Power Analysis of an Automated Dynamic Cone Penetrometer

by C Wesley Tipton IV and Donald H Porschet

Approved for public release; distribution unlimited.

NOTICES

Disclaimers

The findings in this report are not to be construed as an official Department of the Army position unless so designated by other authorized documents.

Citation of manufacturer's or trade names does not constitute an official endorsement or approval of the use thereof.

Destroy this report when it is no longer needed. Do not return it to the originator.

ARL-TR-7494 ● SEP 2015

US Army Research Laboratory

Power Analysis of an Automated Dynamic Cone Penetrometer

by C Wesley Tipton IV and Donald H Porschet
Sensors and Electron Devices Directorate, ARL

Approved for public release; distribution unlimited.

REPORT DOCUMENTATION PAGE	Form Approved OMB No. 0704-0188

Public reporting burden for this collection of information is estimated to average 1 hour per response, including the time for reviewing instructions, searching existing data sources, gathering and maintaining the data needed, and completing and reviewing the collection information Send comments regarding this burden estimate or any other aspect of this collection of information, including suggestions for reducing the burden, to Department of Defense, Washington Headquarters Services, Directorate for Information Operations and Reports (0704-0188), 1215 Jefferson Davis Highway, Suite 1204, Arlington, VA 22202-4302 Respondents should be aware that notwithstanding any other provision of law, no person shall be subject to any penalty for failing to comply with a collection of information if it does not display a currently valid OMB control number

PLEASE DO NOT RETURN YOUR FORM TO THE ABOVE ADDRESS.

1. REPORT DATE *(DD-MM-YYYY)* Sep 2015	**2. REPORT TYPE** Final	**3. DATES COVERED (From - To)** 08/2015

4. TITLE AND SUBTITLE Power Analysis of an Automated Dynamic Cone Penetrometer	**5a. CONTRACT NUMBER**
	5b. GRANT NUMBER
	5c. PROGRAM ELEMENT NUMBER
6. AUTHOR(S) C Wesley Tipton IV and Donald H Porschet	**5d. PROJECT NUMBER**
	5e. TASK NUMBER
	5f. WORK UNIT NUMBER
7. PERFORMING ORGANIZATION NAME(S) AND ADDRESS(ES) US Army Research Laboratory ATTN: RDRL-SED-P 2800 Powder Mill Road Adelphi, MD 20783-1138	**8. PERFORMING ORGANIZATION REPORT NUMBER** ARL-TR-7494
9. SPONSORING/MONITORING AGENCY NAME(S) AND ADDRESS(ES)	**10. SPONSOR/MONITOR'S ACRONYM(S)**
	11. SPONSOR/MONITOR'S REPORT NUMBER(S)

12. DISTRIBUTION/AVAILABILITY STATEMENT

Approved for public release; distribution unlimited.

13. SUPPLEMENTARY NOTES

14. ABSTRACT

We present an analysis of the power requirements of an automated Dynamic Cone Penetrometer (DCP) based on a 16-mm diameter drive rod. The concept system has an estimated weight of 25 kg (not including batteries and rod) and requires eight BA5590 batteries to complete a typical site survey. At an impact rate of 1 Hz, a 100 CBR survey would take approximately 3.6 h of operating time.

15. SUBJECT TERMS

dynamic cone penetrometer, stepper motor

16. SECURITY CLASSIFICATION OF:			**17. LIMITATION OF ABSTRACT**	**18. NUMBER OF PAGES**	**19a. NAME OF RESPONSIBLE PERSON**
					C Wesley Tipton IV
a. REPORT	**b. ABSTRACT**	**c. THIS PAGE**			**19b. TELEPHONE NUMBER (Include area code)**
Unclassified	Unclassified	Unclassified	UU	26	301-394-5209

Standard Form 298 (Rev. 8/98)
Prescribed by ANSI Std. Z39.18

Contents

List of Figures **iv**

List of Tables **iv**

1. Introduction **1**

2. System Description **2**

2.1 Power Source 2

2.2 Hammer Mass 4

2.3 Motor 5

3. Analyses **5**

4. Conclusion **11**

5. References and Notes **13**

Appendix A. Performance Calculation Worksheets **15**

List of Symbols, Abbreviations, Acronyms, and Variables **19**

Distribution List **20**

List of Figures

Fig. 1 Diagrams of the a) conventional and b) automated dynamic cone penetrometer 1

Fig. 2 BA5590 high-capacity battery electrical schematic and package....3

Fig. 3 Discharge characteristic of the SAFT BA5590HC battery[2] a) as a function of temperature and b) as a function of load current at 21 °C ..3

Fig. 4 K33 stepper motor candidate in the standard NEMA 34 package....5

Fig. 5 Analytical geometry of the automated DCP 6

Fig. 6 Estimated relationships between the phase current and torque for several K33 family winding types 8

Fig. 7 Simulated motor speed for an applied phase current for K33 winding types J, M, and K 9

Fig. 8 The influence of hammer mass on the spring compression distance and spring constant based on a maximum motor current of 2.5 A per phase, gear diameter of 31.75 mm, and equal compression and drop distances....10

Fig. 9 The number of impacts delivered per battery pack and charging time as a function of hammer mass based on a maximum motor current of 2.5 A per phase, gear diameter of 31.75 mm, and equal compression and drop distances....11

List of Tables

Table 1 Battery pack configurations using the BA5590HC battery 4

Table 2 Density of selected native materials that could be used for the hammer mass....4

Table 3 Automated DCP performance comparison 11

1. Introduction

Measuring the strength and thickness of soil layers is often performed using a hand-operated Dynamic Cone Penetrometer (DCP). The conventional DCP, shown in Fig. 1a, consists of two 16-mm diameter rods coupled to the anvil. The lower (driven) rod, having a pointed tip, is driven into the soil by dropping the sliding hammer, located on the upper rod, onto the anvil. The penetrating depth per impact may then be correlated to soil strength parameters such as the California Bearing Ratio (CBR). In order to perform the soil strength measurements in a more time-efficient manner, the Army desires an automated DCP (ADCP) system. Furthermore, the driven rod and impulse applied must be similar to that of the conventional equipment and test standard[1] to maintain compatibility with existing survey data.

Fig. 1b shows the cross-section of the concept mechanism used in this assessment of the power requirements of an ADCP. A stepper motor is used to raise the hammer and compress a spring. The spring stores the energy needed to drive the rod and reduces the overall height of the system.

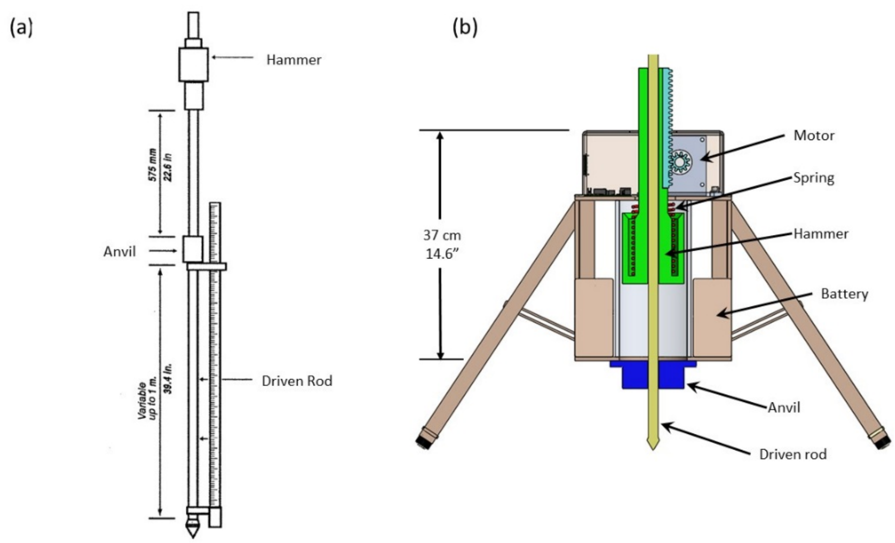

Fig. 1 Diagrams of the a) conventional and b) automated dynamic cone penetrometer

To achieve the required kinetic energy of 45 J, the 8-kg hammer must have a velocity of 3.4 m/s upon impact with the anvil. At this speed, compact stepper motors produce very little output power. In fact, all electromagnetic actuators experience diminished force (or torque) as their armature or rotor speed increases due to the generated back-electromotive force (EMF). In this analysis, we require the motor to produce high power at low shaft speeds to compress the spring. Once the spring is compressed, the motor is de-energized and the hammer accelerates toward the anvil. Energy is transferred from the spring until the hammer reaches the spring's free length. From that point, the hammer is accelerated by gravity only. This approach can also accommodate the testing of weaker materials by allowing the user to vary the compression distance and, subsequently, hammer energy.

2. System Description

There are many design tradeoffs to consider in the selection of the major system components—power source, hammer mass, motor, and spring. In general, we would like the power source to provide a high voltage so that the impact of back-EMF and power loss in the windings are minimized. Increased torque at high speeds will allow the spring to be compressed more quickly and for the strike rate to be increased.

2.1 Power Source

In this analysis, the power source is based on the BA5590 high capacity battery produced by SAFT. This battery is configured, as shown in Fig. 2, as two groups of cells each with a nominal voltage of 15 V, and having a thermal cut-off switch and 3 A fuse. Also, integrated diodes prevent current from being injected into the batteries. In pulsed power applications, the fuse, diode, and thermal switch will limit the peak and average power delivered by the battery. The performance characteristics of the BC5590-HC are shown in Fig. 3. We limit the minimum operating temperature to 0 °C; therefore, each cell group is rated for 13 V at 6 A·h capacity with a maximum current of 2.5 A. The power sources shown in Table 1 are considered assuming the maximum number of batteries used during operation is 4 and by changing the group configuration.

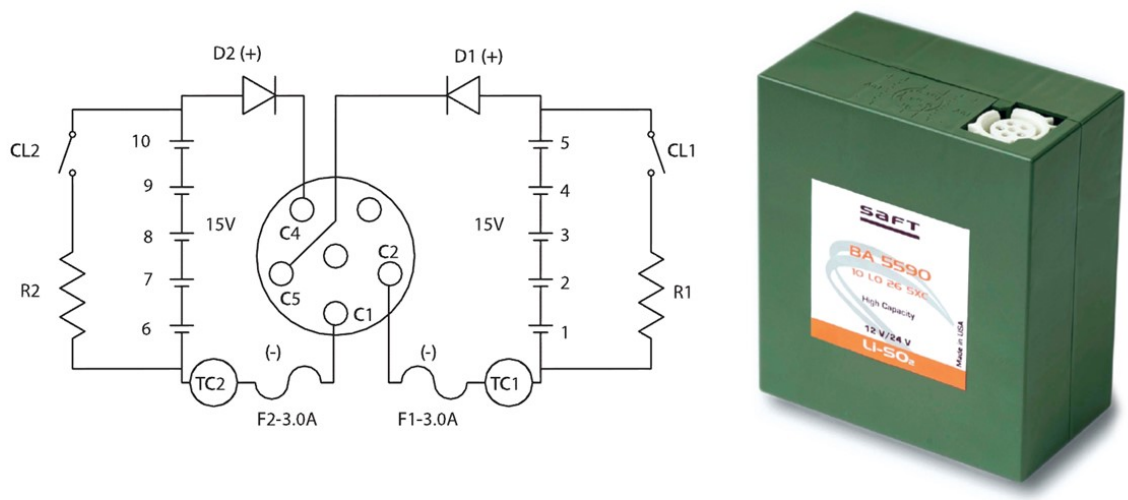

Fig. 2 BA5590 high-capacity battery electrical schematic and package

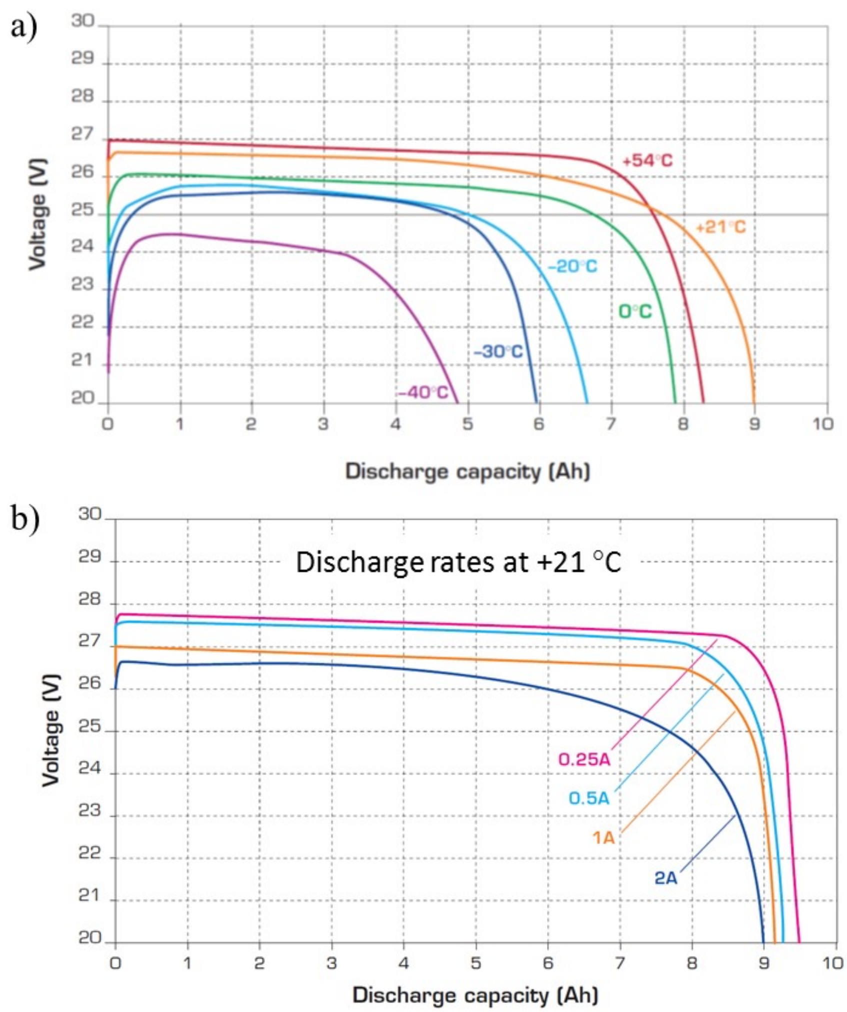

Fig. 3 Discharge characteristic of the SAFT BA5590HC battery[2] a) as a function of temperature and b) as a function of load current at 21 °C

Table 1 Battery pack configurations using the BA5590HC battery

Number of batteries	Cell group Configuration	Output voltage (V)	Maximum current (A)	Capacity (A·h)
4	4-series, 2-parallel	52	5	12
3	3-series, 2-parallel	39	5	12
2	2-series, 2-parallel	26	5	12
4	2-series, 4-parallel	26	10	24

2.2 Hammer Mass

In order to reduce the transportation weight of the ADCP system, the use of native materials for the hammer mass may be desired. Table 2 lists the densities of some common materials.[3] For a target hammer mass of 8 kg, approximately 6.5 L of clay would be needed, necessitating that a container of this volume be integrated into the system. To minimize the system volume, the design presented in this analysis does not use native materials. The hammer, comprised of a striking head and drive shaft, is made of steel.

Table 2 Density of selected native materials that could be used for the hammer mass

Material	kg/liter	kg/m^3	lbs/ft^3
sand	1.52	1520	95
sandy loam	1.44	1440	90
loam	1.36	1360	85
silt loam	1.28	1280	80
clay loam	1.28	1280	80
clay	1.2	1200	75
amphibolite	2.9	2900	181
dolomite	2.8	2800	175
gneiss	2.7	2700	169
limestone	2	2000	125
marble	2.7	2700	169
schist	3	3000	187
shale	2.3	2300	144
slate	2.7	2700	169
pyrite	5	5000	312
lead	11.3	11300	705
steel	7.8	7800	487

2.3 Motor

The Kollmorgen KM-Series of high-torque stepper motors spans a holding torque (τ) range of 0.5 to 30 N·m and includes a variety of winding configurations.[4] These are 2- or 4-phase motors and have a resolution of 200 steps per revolution. From a power density perspective, we would like to use a 2-phase motor (bipolar drive) and, from a performance perspective, a higher voltage, lower current machine. The maximum source current of 5 or 10 A must be divided equally between the phases; therefore, we are limited to a maximum phase current of 2.5 or 5 A. To estimate the required torque, we round the required impact energy to 50 J and estimate a spring constant (k) of 5000 N·m. Since the energy stored in the spring is $\frac{1}{2}kx^2$, the spring force, ($k \cdot x$) is calculated to be 707 N. For a drive gear radius of 12.7 mm, we get an estimated torque of 9 N·m; a range of 10 to 15 N·m will be used.

Based on the current and torque estimates, the subset of K33-motors appears to be a good choice and is packaged as shown in Fig. 4. Within the K33 family, there are 18 different winding configurations. Of these, 6 have a maximum rated current of 2–3 A, with model K33xxLK-L having the lowest winding inductance, and model K33xxLM-L having the lowest inductance among the 5-A-rated motors. In the following analysis, the dynamic performance of these motors will be assessed.

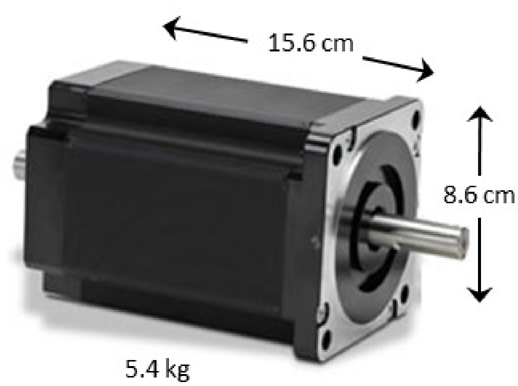

Fig. 4 K33 stepper motor candidate in the standard NEMA 34 package

3. Analyses

Analysis of the mechanical system begins with the calculation of the forces acting on the hammer. Figure 5 shows a diagram of the hammer and anvil with the distance variables needed for the calculations.

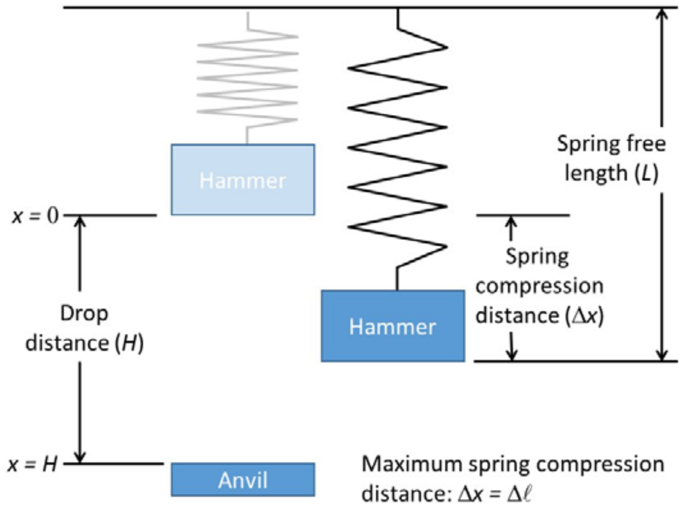

Fig. 5 Analytical geometry of the automated DCP

To discharge the spring, the stepper motor is de-energized and the hammer accelerates towards the anvil under the influence of three entities—gravity, the spring, and the rotational inertia of the motor and gear. There are other frictional forces present, but these are not considered. In the fully charged position, the hammer is subjected to the greatest force, which creates a very large angular acceleration of the rotor once the hammer is released. During this time, the torque generated by the rotor (and gear) are high and tend to decrease the magnitude of the force directed toward the anvil. The total discharging force (F) is expressed as

$$F = m\bar{a} = mg + k(\Delta l - x) - \frac{J\alpha}{r}$$

where m is the mass of the hammer, $\bar{a}$ is the average linear acceleration, g is the gravitational acceleration, k is the spring constant, Δl is the maximum spring compression distance, x is the present compression location, J is the rotor inertia, α is the rotor angular acceleration, and r is the gear radius.

By converting the angular acceleration to linear acceleration and letting $\beta = 1 + {}^{J}\!/_{mr^2}$, the total force may be rewritten as

$$F = \frac{mg + k(\Delta l - x)}{\beta}, \qquad 0 \leq x \leq \Delta l$$

Once the hammer travels past the spring's free length (L), the spring force is zero and total force becomes

$$F = \frac{mg}{\beta}, \Delta l \leq x \leq H$$

Because the force is not constant while the hammer is moving under the influence of the spring, the calculation of the energy gained is not trivial. Therefore, the work performed by the external forces is estimated by

$$W = -\Delta F \Delta x$$

where ΔF is the incremental change in force (decreasing during discharge) for an incremental change in the distance traveled (Δx). Now, using the conservation of energy, the hammer velocity (v) is given by

$$v = \sqrt{\frac{2W}{m}}$$

During charging, the spring is compressed a pre-defined distance of Δl under relatively low accelerating forces and, therefore, the rotational inertia of the electromagnetic system is not considered significant. The motor must generate a torque that counters gravity and the spring at a shaft speed (S) that allows an acceptable impact rate of approximately 1 Hz.

The motor's drive electronics must limit the phase currents in accordance with the battery's capability by adjusting the electrical stepping frequency. This drive frequency and Δx are used to calculate the spring compression time. The discharge time is approximately an order of magnitude smaller than the charge time.

Unfortunately, the manufacturer does not provide the torque vs. phase current (τ-I) characteristics of most of the candidate motors. So, the K33-xxHM motor's curve was normalized and scaled to the motors of interest by using their maximum holding torque and phase current. The estimated characteristics of 4 winding configurations (EJ, LM, LK, and LJ) are given in Fig. 6 and are influenced, primarily, by the number of turns per winding. (The first letter of the 2-letter winding designation denotes bi-polar series (L), bi-polar parallel (H), or unipolar (E) operation, while the second letter denotes the winding's electrical specification. In the following discussion, the LK winding will be referred to as the K-winding, for example, because the operational mode is implied.) Because we are using a low voltage power source with low current capability, we focus our investigation on windings with a high number of turns and that are series-connected. One disadvantage, however, is that these windings have relatively high inductance and, therefore, will have limited high-speed performance.

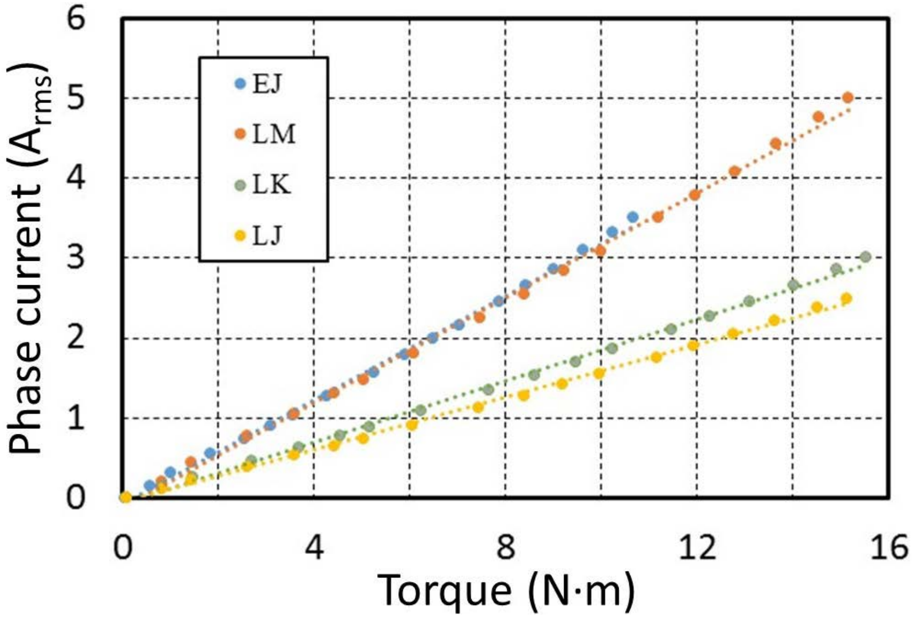

Fig. 6 Estimated relationships between the phase current and torque for several K33 family winding types

Fig. 7 is based on circuit simulations of the phase current (I) using the manufacturer's winding inductance and resistance values. A bipolar, square wave drive signal of several amplitudes (26, 39, and 52 V) and multiple frequencies were used to obtain the root-mean-squared phase currents. Each half-cycle of the applied voltage waveform corresponds to one rotational step, while there are 200 steps per revolution. A back-EMF source was not included in the simulation model because the specifics of each winding configuration was not available. However, a calculation was made of a fourth winding (not considered for this application) whose data was available. In this case, the torque was reduced by 8% at 2000 steps/s and 1% at 400 steps/s. Therefore, the phase current vs. shaft speed (*I*-*S*) curves of Fig. 7 should give a good estimate for our calculations.

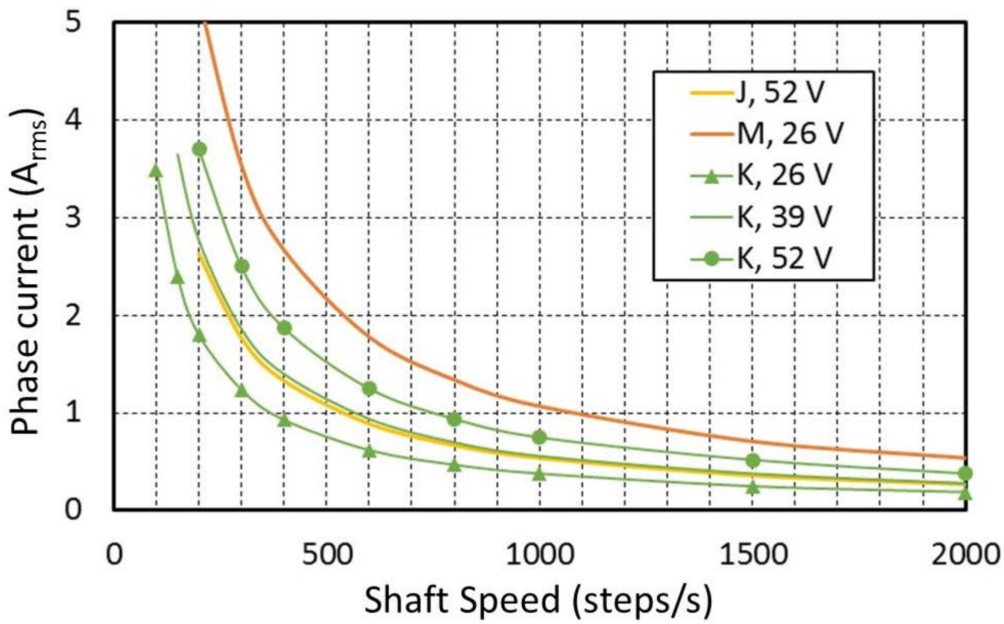

Fig. 7 Simulated motor speed for an applied phase current for K33 winding types J, M, and K

Now that we have the τ-I and I-S relationships, the energy required to compress the spring may be estimated. The average energy needed by the motor during a time interval of the compression process is given as

$$\bar{E} = \frac{\bar{P}\Delta t}{\eta} = \frac{\bar{I}V\Delta t}{\eta} = \frac{\bar{I}V}{\eta}\frac{\Delta x}{\bar{v}}$$

where V is the source voltage, η is the drive efficiency, and $\bar{v}$ is the average linear velocity of the hammer which may be calculated from

$$\bar{v} = \left(\frac{2\pi r}{200}\right)\bar{S}$$

where $\bar{S}$ is the average shaft speed over the time interval of interest.

The motor drive electronics and control algorithm have an impact on the overall system efficiency. At this point, system efficiency is not known. Based on our literature survey, drive efficiency varies between 30% and 70%, and is a function of S. In this analysis, η was assigned a value of 0.3 for $S \leq$ ~300 steps/s and 0.6 for $S \geq$ ~1000 steps/s.

The electromechanical relationships presented were incorporated into a spreadsheet designed to estimate the energy required to execute a charge-discharge event and the time needed to charge the spring. The spreadsheet is used by adjusting m, k, and Δl such that the maximum phase current is not exceeded and the compression distance is minimized. If the compression and drop distances are to be equal, then the hammer must attain 45 J over this distance. Otherwise, the drop distance may be larger than the compression distance and additional energy be gained by gravitational acceleration. Selected copies of the spreadsheet are included in Appendix A for 52, 39, and 26-V operation.

Fig. 8 shows the dependence of Δx and k on m for a maximum phase current of 2.5 A and gear diameter of 31.75 mm. These parameters were adjusted so that the compression distance and drop distance were equal. Note that over a change of 5 kg, the drop height changes by only 4 cm and the spring constant changes by approximately 12% over the same range. In terms of operational performance, Fig. 9 shows the dependence of the battery lifetime and charging time on the hammer mass.

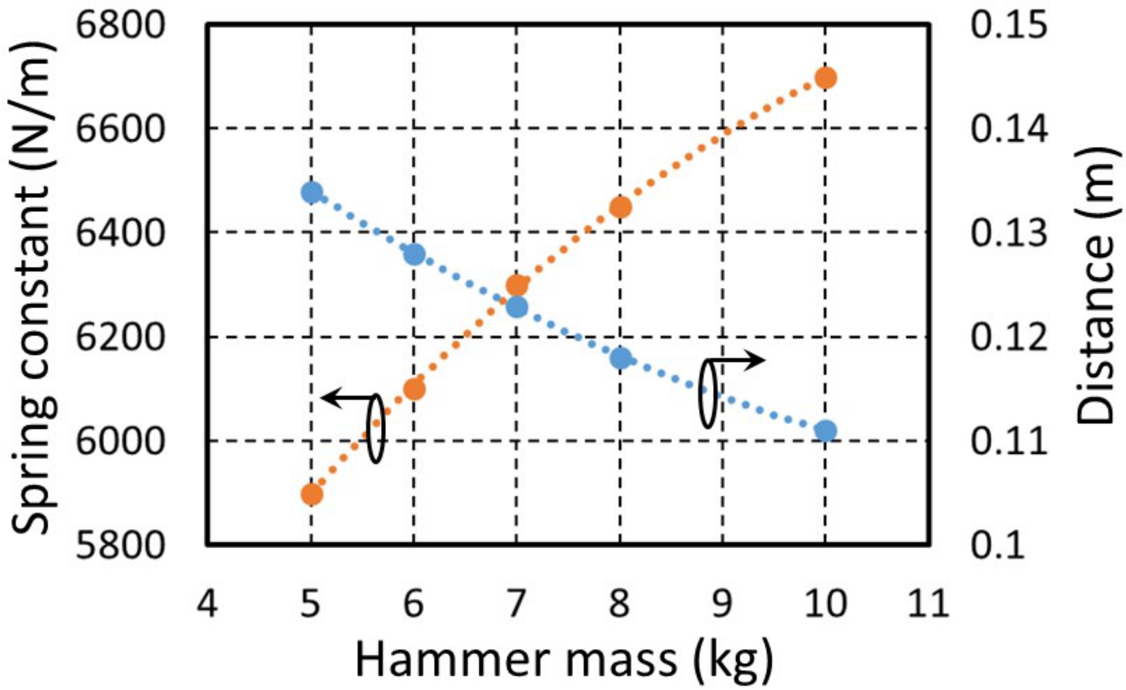

Fig. 8 The influence of hammer mass on the spring compression distance and spring constant based on a maximum motor current of 2.5 A per phase, gear diameter of 31.75 mm, and equal compression and drop distances

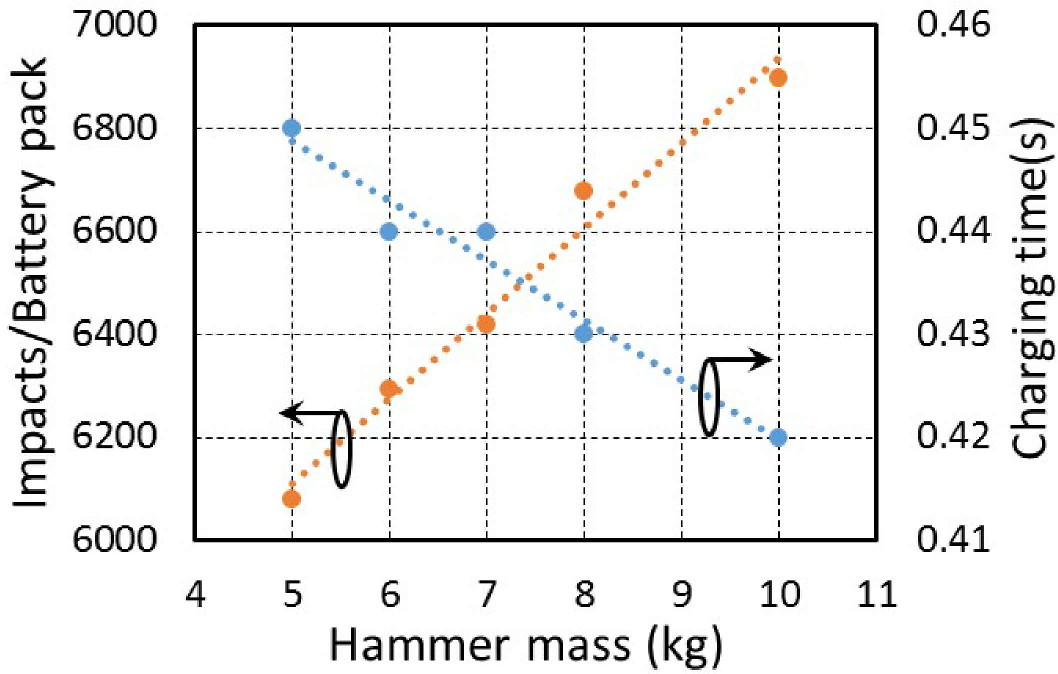

Fig. 9 The number of impacts delivered per battery pack and charging time as a function of hammer mass based on a maximum motor current of 2.5 A per phase, gear diameter of 31.75 mm, and equal compression and drop distances

Table 3 is an expanded version of Table 1 in which the compression time and number of impacts per battery are added. In all cases, the hammer mass is 8 kg. By increasing the battery voltage, the compression time is reduced and the energy per impact is reduced.

Table 3 Automated DCP performance comparison

Number of batteries	Cell group Configuration	Output voltage (V)	Maximum current (A)	Capacity (A·hr)	Compression time (s)	Impacts / battery pack
4	4-series, 2-parallel	52	5	12	0.42	6684
3	3-series, 2-parallel	39	5	12	0.56	4967
2	2-series, 2-parallel	26	5	12	0.67	2599
4	2-series, 4-parallel	26	10	24	0.67	5199

4. Conclusion

Based on this analysis, an automated DCP system using the conventional 16-mm diameter rod is feasible and has an estimated weight of 25 kg (not including batteries and rod). To complete the DCP surveys described by Gregory Fischer[5] using the concept ADCP, 13,024 hammer impacts are needed for a site with a CBR of 100, and 10,649 impacts are needed for one with a CBR of 80. We estimate that eight BA5590 batteries would be needed to complete one survey for either of these cases. At an impact rate of 1 Hz, the 100 CBR survey would take 3.6 h of operating time. As previously stated, the overall system efficiency and, therefore, thermal limitations, are not precisely known at this time. Although capable of 1-Hz operation, the system may have to be operated at lower impact rates to prevent overheating.

The analysis of the automated DCP is based on the conventional hammer-anvil mechanism, wherein the details of the impulse are not needed. If specifics of the force-time profile become available, a follow-on analysis could be made of an electromagnetic impulse generator that emulates the conventional system.

5. References and Notes

1. Standard Test Method for Use of the Dynamic Cone Penetrometer in Shallow Pavement Applications, ASTM International, D6951/D6951M – 09

2. BA 5590 High Capacity Battery Data Sheet. SAFT [accessed 2015 Aug 17]. http://www.saftbatteries.com/battery-search/small-primary-lithium-systems-soldiers

3. Density of Rocks and Soils. ChemPRIME [accessed 2015 Aug 17]. http://wiki.chemprime.chemeddl.org/index.php/Density_of_Rocks_and_Soils

4. Kollmorgen Stepper Solutions Catalog. Kollmorgen [accessed 2015 Sept 2]. http://www.kollmorgen.com/en-us/products/motors/stepper/_literature/stepper-and-synchronous-motors-catalog-en-us-revc/

5. Private communication with Dr. Gregory Fischer of the US Army Research Laboratory. 2015 July 9

INTENTIONALLY LEFT BLANK.

Appendix A. Performance Calculation Worksheets

hammer mass	8 kg				168 J	Charging energy	
gear radius	0.0159 m	Beta	1.20		0.42 s	Compression time	
drop height	0.118 m	mg	78.48				
compression length	0.118 m				401 W	Avg. charging power	
spring constant	6450 N/m	waveform modifier		1.5			
motor inertia	4.00E-04 kgm^2						
					Battery energy		312 Whr
battery capacity	6 Ahr						1,123,200 Joules
battery voltage	52 V						
					Blows/battery pack		6,684

Discharge

Charge

Distance (m)	Total Force (N)	Total Work (J)	Velocity (m/s)	Ang. acel. (rad/s^2)	Total Force* (N)	Stored Energy (J)	Torque (Nm)	Motor current (A)	Max. motor speed (steps/s)	Time (s)	Drive Efficiency	Electrical Energy Used (J)
0	700.9	0.0	0.0	5511	839.6	54.2	13.35	2.49	299	0.075	0.30	46.4
0.0118	637.4	7.9	1.4	5011	763.5	44.7	12.14	2.26	330	0.068	0.30	37.7
0.0236	573.9	15.0	1.9	4512	687.4	36.1	10.93	2.03	369	0.060	0.30	29.9
0.0354	510.3	21.4	2.3	4012	611.3	28.5	9.72	1.79	417	0.053	0.30	23.0
0.0472	446.8	27.1	2.6	3512	535.1	21.7	8.51	1.56	480	0.045	0.40	12.7
0.059	383.2	32.0	2.8	3013	459.0	15.9	7.30	1.33	566	0.038	0.40	8.9
0.0708	319.7	36.1	3.0	2513	382.9	10.9	6.09	1.10	688	0.030	0.40	5.8
0.0826	256.1	39.5	3.1	2014	306.8	6.8	4.88	0.86	876	0.023	0.60	2.2
0.0944	192.6	42.2	3.2	1514	230.7	3.6	3.67	0.63	1205	0.015	0.60	1.0
0.1062	129.1	44.1	3.3	1015	154.6	1.4	2.46	0.40	1920	0.012	0.60	0.4
0.118	65.5	45.2	3.4	515	78.5	0.0	1.25	0.17	2000	0.000	0.60	0.0
0.118	65.5	45.2	3.4	515	78.5	0.0	1.25	0.17	2000	0.000	0.60	0.0
0.118	65.5	45.2	3.4	515	78.5	0.0	1.25	0.17	2000	0.000	0.60	0.0
0.118	65.5	45.2	3.4	515	78.5	0.0	1.25	0.17	2000	0.000	0.60	0.0
0.118	65.5	45.2	3.4	515	78.5	0.0	1.25	0.17	2000	0.000	0.60	0.0
0.118	65.5	45.2	3.4	515	78.5	0.0	1.25	0.17	2000	0.000	0.60	0.0
0.118	65.5	45.2	3.4	515	78.5	0.0	1.25	0.17	2000	0.000	0.60	0.0
0.118	65.5	45.2	3.4	515	78.5	0.0	1.25	0.17	2000	0.000	0.60	0.0
0.118	65.5	45.2	3.4	515	78.5	0.0	1.25	0.17	2000	0.000	0.60	0.0
0.118	65.5	45.2	3.4	515	78.5	0.0	1.25	0.17	2000	0.000	0.60	0.0
0.118	65.5	45.2	3.4	515	78.5	0.0	1.25	0.17	2000	0.000	0.60	0.0

* assumes angular acceleration and motor inertia are not significant

hammer mass	8 kg				170 J	Charging energy
gear radius	0.0159 m	Beta	1.20		0.56 s	Compression time
drop height	0.118 m	mg	78.48			
compression length	0.118 m				302 W	Avg. charging power
spring constant	6450 N/m	waveform modifier	1.5			
motor inertia	4.00E-04 kgm^2					
					Battery energy	234 Whr
battery capacity	6 Ahr					842,400 Joules
battery voltage	39 V					
					Blows/battery pack	4,967

Discharge

Charge

Distance (m)	Total Force (N)	Total Work (J)	Velocity (m/s)	Ang. acel. (rad/s^2)	Total Force* (N)	Stored Energy (J)	Torque (Nm)	Motor current (A)	Max. motor speed (steps/s)	Time (s)	Drive Efficiency	Electrical Energy Used (J)
0	700.9	0.0	0.0	5511	839.6	54.2	13.35	2.49	222	0.101	0.30	46.8
0.0118	637.4	7.9	1.4	5011	763.5	44.7	12.14	2.26	246	0.091	0.30	38.0
0.0236	573.9	15.0	1.9	4512	687.4	36.1	10.93	2.03	274	0.081	0.30	30.2
0.0354	510.3	21.4	2.3	4012	611.3	28.5	9.72	1.79	310	0.071	0.30	23.2
0.0472	446.8	27.1	2.6	3512	535.1	21.7	8.51	1.56	357	0.061	0.40	12.9
0.059	383.2	32.0	2.8	3013	459.0	15.9	7.30	1.33	420	0.051	0.40	9.0
0.0708	319.7	36.1	3.0	2513	382.9	10.9	6.09	1.10	510	0.041	0.40	5.9
0.0826	256.1	39.5	3.1	2014	306.8	6.8	4.88	0.86	648	0.031	0.60	2.2
0.0944	192.6	42.2	3.2	1514	230.7	3.6	3.67	0.63	890	0.021	0.60	1.0
0.1062	129.1	44.1	3.3	1015	154.6	1.4	2.46	0.40	1416	0.014	0.60	0.4
0.118	65.5	45.2	3.4	515	78.5	0.0	1.25	0.17	2000	0.000	0.60	0.0
0.118	65.5	45.2	3.4	515	78.5	0.0	1.25	0.17	2000	0.000	0.60	0.0
0.118	65.5	45.2	3.4	515	78.5	0.0	1.25	0.17	2000	0.000	0.60	0.0
0.118	65.5	45.2	3.4	515	78.5	0.0	1.25	0.17	2000	0.000	0.60	0.0
0.118	65.5	45.2	3.4	515	78.5	0.0	1.25	0.17	2000	0.000	0.60	0.0
0.118	65.5	45.2	3.4	515	78.5	0.0	1.25	0.17	2000	0.000	0.60	0.0
0.118	65.5	45.2	3.4	515	78.5	0.0	1.25	0.17	2000	0.000	0.60	0.0
0.118	65.5	45.2	3.4	515	78.5	0.0	1.25	0.17	2000	0.000	0.60	0.0
0.118	65.5	45.2	3.4	515	78.5	0.0	1.25	0.17	2000	0.000	0.60	0.0
0.118	65.5	45.2	3.4	515	78.5	0.0	1.25	0.17	2000	0.000	0.60	0.0
0.118	65.5	45.2	3.4	515	78.5	0.0	1.25	0.17	2000	0.000	0.60	0.0

* assumes angular acceleration and motor inertia are not significant

hammer mass	8 kg			216 J	Charging energy
gear radius	0.0159 m	Beta	1.20	0.67 s	Compression time
drop height	0.2 m	mg	78.48		
compression length	0.105 m			322 W	Avg. Charging Power
spring constant	8300 N/m	waveform modifier	1.5		
motor inertia	4.00E-04 kgm^2				
				Battery energy	312 Whr
battery capacity	12 Ahr				1123200 Joules
battery voltage	26 V				
				Impacts/battery pack	5199

Discharge

Charge

Distance (m)	Total Force (N)	Total Work (J)	Velocity (m/s)	Ang. acel. (rad/s^2)	Total Force* (N)	Stored Energy (J)	Torque (Nm)	Motor current (A)	Max. motor speed (steps/s)	Time (s)	Drive Efficiency	Electrical Energy Used (J)
0	793.1	0.0	0.0	6235	950.0	61.4	15.10	4.96	213	0.094	0.30	57.83
0.0105	720.4	7.9	1.4	5663	862.8	51.9	13.72	4.51	235	0.085	0.30	47.18
0.021	647.6	15.1	1.9	5091	775.7	43.3	12.33	4.05	261	0.076	0.30	37.61
0.0315	574.8	21.5	2.3	4519	688.5	35.6	10.95	3.60	295	0.067	0.30	29.13
0.042	502.1	27.2	2.6	3947	601.4	28.9	9.56	3.14	338	0.057	0.40	16.30
0.0525	429.3	32.1	2.8	3375	514.2	23.0	8.18	2.69	396	0.048	0.40	11.56
0.063	356.6	36.2	3.0	2803	427.1	18.1	6.79	2.23	477	0.039	0.40	7.63
0.0735	283.8	39.6	3.1	2231	339.9	14.0	5.40	1.78	600	0.030	0.60	3.00
0.084	211.0	42.2	3.2	1659	252.8	10.9	4.02	1.32	809	0.021	0.60	1.46
0.0945	138.3	44.0	3.3	1087	165.6	8.7	2.63	0.87	1239	0.015	0.60	0.64
0.105	65.5	45.1	3.4	515	78.5	7.5	1.25	0.41	1500	0.013	0.60	0.34
0.1145	65.5	45.7	3.4	515	78.5	6.7	1.25	0.41	1500	0.013	0.60	0.34
0.124	65.5	46.3	3.4	515	78.5	6.0	1.25	0.41	1500	0.013	0.60	0.34
0.1335	65.5	46.9	3.4	515	78.5	5.2	1.25	0.41	1500	0.013	0.60	0.34
0.143	65.5	47.6	3.4	515	78.5	4.5	1.25	0.41	1500	0.013	0.60	0.34
0.1525	65.5	48.2	3.5	515	78.5	3.7	1.25	0.41	1500	0.013	0.60	0.34
0.162	65.5	48.8	3.5	515	78.5	3.0	1.25	0.41	1500	0.013	0.60	0.34
0.1715	65.5	49.4	3.5	515	78.5	2.2	1.25	0.41	1500	0.013	0.60	0.34
0.181	65.5	50.1	3.5	515	78.5	1.5	1.25	0.41	1500	0.013	0.60	0.34
0.1905	65.5	50.7	3.6	515	78.5	0.7	1.25	0.41	1500	0.013	0.60	0.34
0.2	65.5	51.3	3.6	515	78.5	0.0	1.25	0.41	1500	0.013	0.60	0.34

* assumes angular accelleration and motor inertia are not significant

List of Symbols, Abbreviations, Acronyms, and Variables

CBR	California bearing ratio
DCP	dynamic cone penetrometer
EMF	electromotive force
NEMA	National Electrical Manufacturers Association

1 DEFENSE TECH INFO CTR
(PDF) DTIC OCA

2 US ARMY RSRCH LAB
(PDF) IMAL HRA MAIL & RECORDS MGMT
RDRL CIO LL TECHL LIB

1 GOVT PRNTG OFC
(PDF) A MALHOTRA

9 US ARMY RSRCH LAB
(PDF) RDRL SED C
W TIPTON
RDRL SED
E SHAFFER
RDRL SED P
D PORSCHET
D URCIUOLI
H O'BRIEN
M HINOJOSA
R THOMAS
RDRL SES X
G FISCHER
J HOPKINS